Chemically Functionalizing Controlled Dielectric

Breakdown Silicon Nitride Nanopores by Direct

Photohydrosilylation

Y. M. Nuwan D. Y. Bandara,† Buddini I. Karawdeniya,† James T. Hagan, Robert B. Chevalier, and Jason R. Dwyer*.

Department of Chemistry, University of Rhode Island, 140 Flagg Road, Kingston, RI, 02881, United States.

KEYWORDS Nanopore surface chemistry; hydrosilylation; silane chemistry; nanopore conductance; click chemistry; monolayer formation; silicon nitride

Abstract. Nanopores are a prominent enabling tool for single-molecule applications such as DNA sequencing, protein profiling, and glycomics, and the construction of ionic circuit elements. Silicon nitride (SiN_x) is a leading scaffold for these <100 nm-diameter nanofluidic ion-conducting channels, but frequently challenging surface chemistry remains an obstacle to their use. We functionalized more than 100 SiN_x nanopores with different surface terminations—acidic (Si-R-OH, Si-R-CO₂H), basic (Si-R-NH₂), and nonionizable (Si-R-C₆H₃(CF₃)₂)—to chemically tune the nanopore size, surface charge polarity, and subsequent chemical reactivity, and to change their conductance by changes of solution pH. The initial one-reaction-step covalent chemical film

formation was by hydrosilylation, and could be followed by straightforward condensation and click reactions. The hydrosilylation reaction step used neat reagents with no special precautions such as guarding against water content. A key feature of the approach was to combine controlled dielectric breakdown (CDB) with hydrosilylation to create and functionalize SiN_x nanopores. CDB thus replaced the detrimental but conventionally necessary surface pretreatment with hydrofluoric acid. Proof-of-principle detection of the canonical test molecule, λ -DNA, yielded signals that showed that the functionalized pores were not obstructed by chemical treatments, but could translocate the biopolymer. The characteristics were tuned by surface coating character. This robust and flexible surface coating method, freed by CDB from HF etching, portends the development of nanopores with surface chemistry tuned to match the application, extending even to the creation of biomimetic nanopores.

Introduction. Nanopores offer a broad range of standout capabilities for single molecule science.¹⁻⁶ They can serve as the integral element of single-molecule sensors and force microscopes; as ionic and fluidic circuit elements; and in a host of roles that exploit the rich diversity of function that can emerge from a nanoscale channel through a thin membrane (Figure 1).^{2, 5-11} The need for robust, size-tuneable nanopores compatible with conventional (nano)fabrication workflows makes thin-film, low-pressure chemical vapour deposition (LPCVD) silicon-rich silicon nitride (SiN_x) a popular material choice.^{2, 5, 12} This is in spite of often unfavourable native surface chemistry that can lead to pore clogging, or require complex, expensive, or unreliable surface functionalization strategies to compensate.^{2, 5, 13-16} Silanized nanopores have been reported, but have gained little traction in the field because of difficulties

controlling the reaction and necessary SiN_x surface chemistry quality, especially within a confined volume.^{2,5,14,17} Without scrupulous control over reaction conditions that can be difficult to achieve on open surfaces, let alone inside a nanopore, unwanted processes such as polymerization could easily close the pores to analyte translocation.

Covalent coupling of carbon to silicon-rich SiN_x by hydrosilylation has been shown to be robust, reliable, and flexible in performance on planar films (and extended to the curved surface of a microsieve) prepared by hydrofluoric acid etching.^{2, 18-22} Terminal alkenes and alkynes can be conveniently photochemically or thermally linked to SiN_x to form monolayers capable of possessing a wide variety of terminal functional groups amenable to an array of subsequent surface chemical modifications.^{2, 18-21} Two such reactions—condensation and click—provide simple; and fast, catalyst-free, facile, high yielding and quantitative, byproduct-free reactions, respectively, with both true to an ethos of low-barrier surface functionalization.²³⁻²⁴ The literature emphasizes that hydrosilylation should deliver no more than a monolayer of coverage, 18-21, 25 while still acknowledging the possibility for photoexposure-dependent creation of thicker, although still <10 nm-thick films by a mechanism that remains unclear. 19 The subsequent condensation and click reactions proposed to extend the initial photohydrosilylated layer are conventional and should not add more than an additional molecular layer. Such controlled chemical flexibility inside of a nanopore would lay the foundation for the pursuit of a myriad of eventual purposes including biomimetic solid-state nanopore creation; nanopore size-tuning using discrete molecular building blocks; nanopore surface passivation; and ionic and molecular transport control through the nanopore.^{2, 5-11, 15-17, 26}

Hydrosilylation has been used to prepare microfilters through SiN_x membranes for biofunctionalization via antibody attachment, allowing selective filtration in complex media with

reduced fouling.²² The key hurdle to adopting hydrosilylation for SiN_x nanopore modification is that the necessary first step is removal of the (native) oxide layer using a hydrofluoric acid etch. 18-²¹ In the ~450 nm-diameter pores of the microfilter, ²² such chemical etching would have minimal consequence on the final pore size. In a much smaller nanopore, though, such an etching step could cause detrimental, even ruinous, pore growth to where the final pore size exceeded the small size needed for single-molecule sensing. We hypothesized that controlled dielectric breakdown (CDB)—a low-overhead approach that has invigorated thin-film nanopore fabrication^{2, 27-28} might expose previously bulk SiN_x for hydrosilylation and thereby eliminate the need for the HF etch step. In brief, in CDB high electric field strengths (<1 V/nm) applied across a SiN_x membrane generate a defect-mediated leakage current prior to dielectric breakdown and the onset of ionic current. This is followed by a continued growth of the nanopore, by unclear mechanism, in response to an applied voltage and mediated by supporting electrolyte composition. With automated feedback control, nanopores no larger than 2 nm in diameter, and up to and greater than 10 nm, can be formed.²⁷ The nature of the surface chemistry of these nascent nanopores is uncertain, and undeniably challenging to ascertain by conventional methods. To explore whether the surface would permit photohydrosilylation, we undertook the reaction outcomes, themselves, as a probe of the surface. We attempted to hydrosilylate SiN_x nanopores formed by CDB with – OH and -NH₂-terminated functional groups, before attempting condensation and click reactions to terminate the initial organic coatings with -CO₂H and -Ph(CF₃)₂ moieties, respectively (Figure 2). Nanopore conductances were recorded as a function of pH, and Equations (1) and (3) were used to recover nanopore surface pK_a and apparent size change with chemical treatment. Finally, λ -DNA was sensed using unfunctionalized and hydrosilylated nanopores at fixed pH to determine

if the functionalized pores remained capable of translocation-based sensing, and to detect any chemically-derived signal differences.

Theory.

Nanopore surface chemical functionalization would change the physical nanopore radius by (at most) the length of the newly installed molecule and its covalent bond to the surface, and the chemistry explored here would produce Si-R-OH, Si-R-CO₂H, Si-R-NH₂, and Si-R-Ph(CF₃)₂ terminal groups (versus the SiN_x surface chemistry of the bare pore²). Characterization of the nanopore and solution interface is conveniently done by measurements of the nanopore conductance (*G*) in electrolyte solution²⁸⁻³⁰

$$G = K \cdot \frac{\pi r_0^2}{l} + \mu |\sigma| \cdot \frac{2\pi r_0}{l} \tag{1}$$

where K is the bulk solution conductivity, r_0 and L are the radius and length of the cylindrical nanopore (a shape suitable for CDB²⁷⁻²⁸), and σ is the nanopore surface charge density that attracts counterions of mobility, μ . The mobilities of potassium and chloride ions are nearly identical so that the changes in the nanopore conductance as the surface charge polarity is changed arise predominantly from the change in σ . The surface conductance term, $\mu|\sigma| \cdot \frac{2\pi r_0}{L}$, is vital in explaining the conductance behavior of nanopores with charged surfaces. ^{2, 28-31} This conductance equation, and variants, have been extensively validated for bare SiN_x in conjunction with complementary techniques, most commonly based on electron microscopy. ^{2, 28-32} Electron-microscopy-based techniques face particular challenges when the imaging target is an organic film coating a nanopore, though: high risks for coating destruction and surface contamination, and the low electron scattering cross-section of carbon (and low contrast with SiN_x). Thus, conductance-based profiling is preferable for evaluating surface coatings: it offers a straightforward, (ideally) nondestructive measurement of nanopore size using the same experimental configuration as

nanopore-based resistive-pulse sensing, and gentle but direct probing of nanopore surface chemistry. The form in Equation (1) conveniently reveals the effects of changes of nanopore surface chemistry—increases in the surface charge density magnitude lead to increases in the conductance—while remaining in good accord with independent nanopore characterizations. 28,30 , $^{32-35}$ The key aspect that we use here for analysis is that for a surface terminated in an ionizable moiety such as Si-R-OH, $\sigma = \sigma(pK_a, pH)$ because of an acid-base equilibrium

Si-R-OH (
$$\sigma = 0$$
) \rightleftharpoons Si-R-O⁻ ($|\sigma| > 0$) + H^+ ; $pK_a \cong -\log([Si-R-O^-][H^+]/[Si-R-OH])$ (2)

(with an analogous expression for a base). Changes of electrolyte pH thus change the magnitude of nanopore surface protonation and imprint the surface coating chemistry (captured in terminal group acid dissociation constant, pK_a) onto the variation of the nanopore conductance with solution pH: $dG/dpH \propto d|\sigma|/dpH$. A convenient closed-form expression to approximate the surface charge density, derived from underlying equations^{31, 36-37} is

$$|\sigma| \cong \frac{C_{\text{eff}}}{\beta e} W\left(\frac{\beta e}{C_{\text{eff}}} \exp\left((pH - pK_a)\ln(10) + \ln(e\Gamma)\right)\right)$$
 (3)

with e the elementary charge, Γ the number of surface chargeable groups, β the inverse of thermal energy, $C_{\rm eff}$ an effective Stern layer capacitance, and W the Lambert W function; the expression used for a base replaces $(pH - pK_a)$ with $-(pH - pK_b)$.

Nanopore surface properties can moderate analyte sensing characteristics. Surface chemical functionalization offers the prospect of control over this phenomenon, with the possibility that uncontrolled or unwanted reactions prevent molecular translocation because of pore clogging as a generally undesirable extreme. In the familiar translocation-based sensing framework, passage of the canonical test molecule, λ -DNA, through the nanopore alters the nanopore conductance by volume exclusion (with cross-sectional radius $r_{\lambda-\text{DNA}}$ for the fully-extended biopolymer) and, by its charged nature, inducing the passage of surface counterions through the nanopore:^{7,8}

$$\Delta G_{\lambda-DNA} = G - G_{\lambda-DNA} = G - \left(K \cdot \frac{\pi}{L} \left(r_0^2 - r_{\lambda-DNA}^2\right) + \mu |\sigma| \cdot \frac{2\pi r_0}{L} + \mu \cdot \frac{q_{\lambda-DNA}}{L}\right)$$

$$= \frac{1}{L} \left(K \cdot \pi r_{\lambda-DNA}^2 - \mu \cdot q_{\lambda-DNA}\right) \tag{4}$$

where G is the open-pore (unblocked) conductance of a nanopore of radius r_0 (see Equation (1)), and $G_{\lambda-DNA}$, $r_{\lambda-DNA}$, and $q_{\lambda-DNA}$ are the nanopore conductance during λ -DNA translocation, the cross-sectional radius of the linearized biopolymer, and its effective linear charge density (here, -0.96 nC m⁻¹).^{29, 38} The conformational flexibility of the λ -DNA allows it to be folded when passing through sufficiently large nanopores; in such cases $\Delta G \sim n\Delta G_{\lambda-DNA}$, where *n* is an integer.³⁹ The observation of characteristic blockages can be used to profile nanopore properties, but it is also a key step when assessing whether or not a chemically modified nanopore remains functional as a translocation-based sensor element. The passage of a charged molecule through a nanopore is affected prominently by electrophoresis and by nanopore surface-mediated effects such as electroosmosis and direct electrostatic interactions. Chemical control over specific and nonspecific nanopore-molecule interactions has manifested in outcomes including translocation selectivity, enhanced molecular flux, and decreased likelihood of nanopore clogging. 15, 17, 39-46 In the context of SiN_x nanopore surface chemistry, there are two paradigms of particular interest for controlling ionic conductance and molecular translocation: control of native surface charge by solution pH, and control by surface modification (with and without accompanying changes of solution pH). 17, 26 The polarity of the nanopore surface charge—native SiN_x is amphoteric²—can be tuned to not only control surface-molecule electrostatics, but also whether electrophoresis and electroosmosis are cooperative or competitive. 12,26 It has been reported that amine-termination of SiN_x pores with 3-(aminopropyl)trimethoxysilane, for example, allowed for the translocation time of 1 kbp DNA to be tuned by a factor of 4 across pH 6, 7, and 8. In brief, the DNA translocation time increased with increasing solution acidification that caused an increase in cationic surface charge density.¹⁷

The change in translocation time with surface charge was ascribed to the predominance of the electrostatic interaction.

While DNA sensing remains a prominent focus of nanopore science, nanopore-based single-molecule sensing has much broader applicability, extending in the biopolymer realm, alone, to include proteins and glycans.⁴⁷ These two classes of analyte have a far greater diversity than DNA, whether viewed from the perspective of molecular structure, size, or molecular charge—including the pH-dependence of molecular charge. Thus, while we use λ -DNA as a test of whether the functionalized pores will support translocation, analyte scope transcends nucleic acid oligomers and polymers. The trend of conductance versus pH is therefore not just a probe of the nanopore surface chemistry, it is a functional demonstration of whether the nanopore surface chemistry can be tuned for compatibility with different analyte properties and interaction mechanisms. For analyte-free applications such as ionic circuit construction, the trend of G versus pH is an assay of the properties of the nanopore as an ionic circuit element.

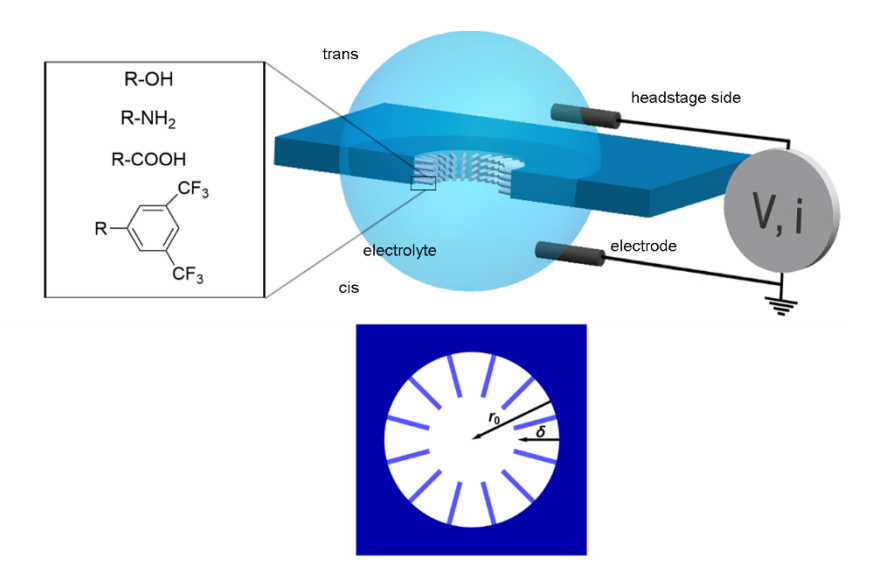


Figure 1. Schematic of the nanopore setup. Molecular coatings inside the nanopore formed through the thin $\mathrm{SiN_x}$ membrane would affect the nanopore size and passage of molecules through the pore. The inset shows the expected terminal groups of reagents used to form the surface coatings. The top-down view at the bottom of the graphic provides a simplified view showing the radius, r_0 , of a $\mathrm{SiN_x}$ nanopore and the thickness, δ , of a schematic organic layer projecting into the pore. The radius of the functionalized nanopore thus becomes $r_0 - \delta$.

Results and Discussion.

CDB was carried out using 1 M KCl electrolytes buffered to pH~7 with HEPES. All nanopores, before and after chemical treatments, produced Ohmic conductance in that same electrolyte composition across the -200 to +200 mV range used for measurements. The well-established surface pretreatment for hydrosilylation of SiN_x is 2 minutes of soaking in 2.5% (v/v) hydrofluoric acid. Nanopore conductances increased after exposure of six independent newly formed SiN_x nanopores to 2.5% (v/v) hydrofluoric acid for a time not exceeding 60 s. The etch rate calculated from these measured nanopore conductances and Equation (1) was~4.4 nm/min. This is unacceptably high as a surface pretreatment for nanopores where preservation of the (small) diameter is paramount for performance, in particular when considering the time necessary to flush out all residual etchant from the pore. We thus directly attempted UV-induced hydrosilylation of SiN_x pores freshly formed by CDB (with no greater than 10 minutes allowed to elapse between

pore formation and optical exposure), without preliminary HF etching. For economy of presentation, we will refer to presumptively functionalized pores as functionalized pores.

The trend of nanopore conductance versus solution pH changed after each chemical treatment carried out (Figure 2), correlated with the expected behaviour of the relevant acidic and basic terminal groups in the 1 M KCl, 10 mM HEPES variable-pH electrolytes. Native SiN_x surfaces present a mixture of amine and silanol groups at the nanopore-solution interface, so that the overall surface charge is determined by the particular SiN_x stoichiometry, by the individual acid-base equilibrium constants (pKa), and by the solution pH.2, 26, 29-31, 36 The SiNx film stress during synthesis is generally measured instead of the underlying stoichiometry, but it should be siliconrich (Si_{3+XS}N₄ with XS>0, close to 1:1 stoichiometry) in order to form a free-standing membrane such as those used here.^{2, 48} The specific stoichiometry of any particular SiN_x membrane is known to be both age- and process-dependent and may be variable from surface into interior, but given the presence of the functional groups noted, the surface charge is positive in acidic pH due to amine protonation, negative in basic pH due to silanol deprotonation (Equation (2)), and neutral at the isoelectric point. The conductance is a minimum at the isoelectric point when $\sigma=0$ (~4.3±0.3, 3 unique pores), and when the pore surface is charged, the surface conductance term in Equation 1, $\mu|\sigma|\cdot\frac{2\pi r_0}{L}$, increases the total nanopore conductance compared to the bulk-only value at the isoelectric point (Figure 2a). Importantly, familiar SiN_x surface chemistry may not reflect the nature of the nanopore surface chemistry immediately upon dielectric breakdown or during subsequent pore enlargement. The nature of SiN_x surface chemistry is well-known to be dependent upon stoichiometry and process conditions: 2 CDB is initiated at defects 27 which implies a different initial localized material composition than elsewhere in the thin film (with film stoichiometry often established by measurements of film stress rather than by directly chemically sensitive methods²,

⁴⁸), and breakdown followed by voltage-assisted pore enlargement involves material removal that most assuredly fits the umbrella of material processing that could further alter surface chemistry. The use of conventional surface science techniques to explore the surface chemistry of a nanopore interior—even if the surface chemistry were unchanging—would be daunting. The outcome of the photohydrosilylation reaction, itself, is thus used to establish whether the HF-free approach of using CDB to create a suitable surface for photohydrosilylation is feasible.

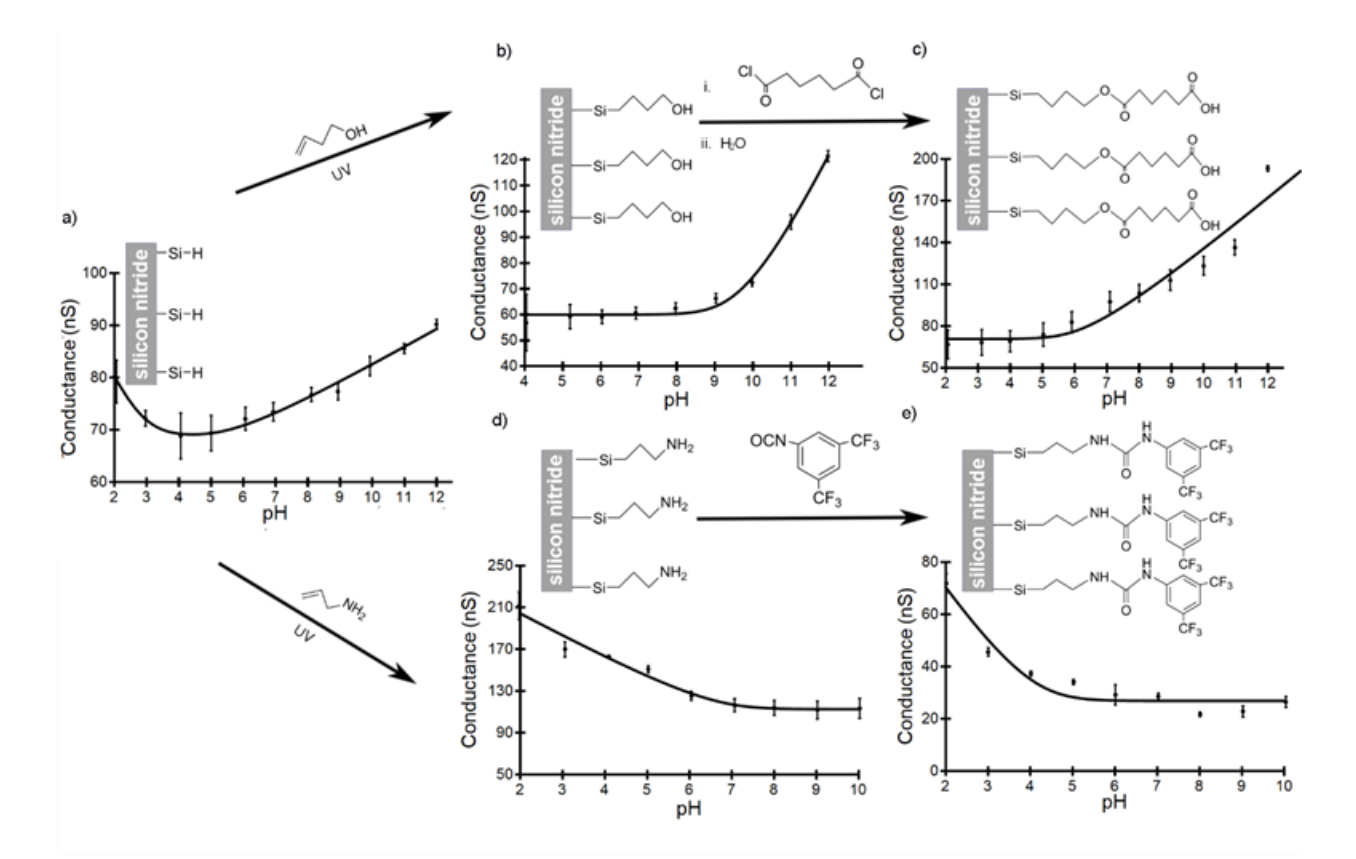


Figure 2. Photohydrosilylation and further chemical transformation of SiN_x nanopores (r_0) tune conductance with pH. Conductance vs. pH profiles of SiN_x nanopores (a) after fabrication by controlled dielectric breakdown process (4.6±0.7 nm); (b) after UV mediated hydrosilylation of 3-butene-1-ol on a pristine SiN_x surface (3.9±0.1 nm); (c) after hydrosilylation with the alcohol and condensation reaction with adipoyl chloride (4.6±0.2 nm); (d) after hydrosilylation with allylamine

(5.7±0.2 nm); and (e) after hydrosilylation with the amine and click reaction with 3,5-bis(trifluoromethyl)phenyl isocyanate (2.6±0.1 nm). Acidic (b) and basic (d) terminal groups produce opposite slopes. The progression from (b) to (c) and (d) to (e) are by modification of an already functionalized surface. Solid traces in each of the graphs are fits (Equation (1) and (3)) to the data. The curves are representative examples drawn from independent trials with the error bar at each pH equal to three times the standard error of the conductance fit from -200 to +200 mV. Nanopore formation and characterization were all carried out in a pH~7 electrolyte consisting of 1 M KCl and 10 mM HEPES.

The conductance versus pH curves of nanopores subjected to HF-free hydrosilyation reaction conditions using 3-butene-1-ol and allyamine showed opposite $\frac{dG}{dpH}$ (Figure 2b,d). For the hydroxyl-terminated nanopore, the Si-R-OH surface equilibrium in Equation (2) would be expected to generate a neutral nanopore in sufficiently acidic solutions. With solution pH sufficiently below the pK_a, the conductance would thus be dominated by the bulk term and be essentially unchanging with pH $(d|\sigma|/dpH\sim0)$ until appreciable surface deprotonation introduced the σ -weighted surface conductance term. For the amine-terminated pore, the equilibrium Si-R-NH₂ ($\sigma = 0$) + H⁺ \rightleftharpoons Si-R-NH₃⁺($|\sigma| > 0$) would show the opposite trend, with surface charging occurring in increasingly acidic solutions. In general, surface attachment can shift the pK from their values in bulk solution owing to a number of factors including distance to the surface and crowding.⁴⁹⁻⁵⁸ A fit to the data for the two coatings using Equations (1) and (3) yielded reasonable values for the surface groups of pK_a~10.5±1.2 (3 unique nanopores), and pK_b~5.2±0.7 (3 unique pores). The opposite relationship between dG/dpH for acid- and base-terminated

nanopore surfaces was fully consistent with expectation. We observed that the amine functionalized pores did not wet as readily as the hydroxyl functionalized ones, though, and had to be left overnight in water prior to conductance measurements. Earlier work outside the nanopore milieu has been carried out using chemically protected terminal amines to guard against the potential photoattachment of the amine terminus to the SiN_x surface.^{20,59} With no such precaution here, those allyamine molecules that coupled to the surface through their amine terminus would expose a hydrophobic alkene group with $\frac{dG}{dpH} = 0$ to the interior, and those that coupled at their alkene terminus would expose a basic amine group with $\frac{dG}{dpH}$ < 0. The observed wetting behavior and trend of conductance with pH were consistent with the formation of a mixed monolayer arising from these two different modes of attachment. Chemical reactivity (below) offers a potential further means to assay the surface chemistry after this first functionalization step. In essence, chemical reactions that will succeed—as measured by suitable change in G and dG/dpH—if the first reaction successfully installed the terminal functional group participating in the reaction, can be used to determine the success of the first reaction. We analyzed the conductance to determine the change in nanopore radius, δ , accompanying the reactions. The radii of SiN_x nanopores before (r_0) and after $(r_0-\delta)$ chemical treatment were calculated using conductance data at pH \sim 7 as described in the Methods and using L (and $L_{\text{eff}} = L/2$, with the 10 nm nominal membrane thickness as the nominal channel length, L)³⁴. For the first chemical functionalization, r_0 , was the radius of the CDB pore. The best-fit values (Figure S-2), with standard errors of the fits, were $\delta \sim 0.87 \pm 0.05$ nm (0.55 \pm 0.04 nm) for the 3-butene-1-ol step (35 unique pores; expected length ~0.7 nm by fully extended chain length normal to the surface), and δ ~2.5±0.1 nm (1.7±0.1 nm) for the allyamine step (32 unique pores). The calculated thickness of the allylamine layer exceeded the estimated upright chain length of ~0.6 nm, suggesting other factors such as multilayer formation, or the need to introduce additional terms into Equation (1) addressing, for example, phenomena related to the longer observed wetting times. 1 H NMR spectra of as-supplied allylamine and of an aliquot that had been subjected to 3 hours of UV exposure revealed no differences, so that unwanted UV-induced side reactions that might result in thicker films by insolution chain extension were likely absent. The possibility of multilayer formation has, though, been reported under these reaction conditions, with similar limitations of extent. 19 Crucially, nanometer resolution over pore dimension is not compromised here. At the pH \sim 7 of the measurement in 1 M KCl electrolyte, Figure 2 (σ by fit) indicated that the SiN_x nanopores were net negatively charged ($\sigma\sim0.03$ C/m²), the -OH-functionalized nanopores were slightly negative (~0.003 C/m²), and the -NH₂-functionalized nanopores were slightly positively charged (~0.008 C/m²). The latter charge density is ~3 times the upper bound, under similar electrolyte conditions (from nanoparticle surface charge measurements), suggested for smaller (~6 nm) SiN_x pores functionalised by silane chemistry. 17

We subjected the ostensibly –OH- and –NH₂-terminated nanopores to further chemical reaction conditions suited to each terminal group: condensation and click, respectively. The –OH-terminated nanopore was reacted with adipoyl chloride (10% v/v in toluene) and then with water (Figure 2c) to generate a carboxylic-acid-terminated surface. The –COOH-terminated nanopore, expected to be more acidic than the –OH-pore, had a faster onset of $\frac{dG}{dpH} \neq 0$, and a pK_a from Equation (1) of ~7.5±0.2 (2 unique pores). The surface pK values for –COOH- (pK_a~7.5±0.2) and –NH₂-terminated (pK_b~5.2±0.7) layers were shifted compared to typical bulk values⁶⁰ of pK_a~3.8–4.8 and pK_b~3.5 (propyl amine), indicating in both cases a lesser charge carried by the surface species than would be carried in solution.⁵³ The case is less definitive for the –OH-terminated surface, but suggestive of a shift in pK_a opposite to that of the –COOH surface, with pK_a~10.5±1.2

versus pK_a~11 by titration of an aqueous solution of butanol (pK_a~15.5 for ethanol⁶⁰). Extensive systematic study may allow such trends to be used to more deeply explore interfacial phenomena within the nanopore setting.⁵¹⁻⁵⁸. The change in nanopore radius for the carboxylic acid-terminated layer with respect to pristine SiN_x using Equation (1) with L (where the nominal value is the 10 nm nominal membrane thickness) and $L_{\rm eff}$ were δ ~2.4±0.1 nm and ~1.7±0.1 nm (17 unique nanopores) respectively, versus the estimated upright thickness of ~1.6 nm.

Beyond providing a counterpoint to the -OH surface termination, amine-terminated nanopores were a necessary starting point for the proposed click reaction. The pores of Figure 2d were treated with neat 3,5-bis(trifluoromethyl)phenyl isocyanate and rinsed with dichloromethane and ethanol, with the fluorine-rich reagent used to ensure rapid reaction rates. We anticipated that this treatment would result in slow wetting arising from the hydrophobicity of the outermost fluorinated aromatic ring. Overnight soaking seemed sufficient to wet the pores, with no further changes in conductance noted for an additional 48 hours of soaking time. Absent an ionizable terminal group, we further expected that the conductance versus pH curve would be flat (bulk-only). The measured curve (Figure 2e), though, qualitatively resembled that of the allylamine-terminated SiN_x. Use of the pH \sim 7 conductance data before and after the click reaction with L ($L_{\rm eff}$) gave a $\delta \sim$ 5.4 \pm 0.3 nm (~3.7±0.2 nm) change in radius (8 unique nanopores), lending credence to the successful installation of a surface species, although the radius change was larger than the ~1.2 nm expected based on molecular length, alone. Fits to the conductance versus pH curves yielded a surface pK_b of ~3.6±0.7 (3 unique nanopores). This value reveals a change in surface chemistry compared to the allylamine base layer, supporting a surface chemical change after the click reaction in spite of the somewhat similar appearance of the G versus pH curve. The surface chemistry of Figure 2e, however, was more complex than merely termination with a species without a terminal ionizable

group. Steric hindrance or terminal alkenes in the initial layer may limit the achievable surface coverage so that SiN_x amine sites remained unreacted and contributed to the surface conductance from underneath a more hydrophobic pocket. Such solvation effects⁵² are not accounted for in Equation (1), so that the derived nanopore radius would be in error. The surface linker also contains NH moieties that could participate in acid-base equilibria, underneath the nonionizable terminal group, to generate a surface conductance term with the appropriate slope dG/dpH. A number of important points drawn from across the multiple surface modification reactions deserve emphasis. First, the ability to chemically transform the initial photohydrosilylated layers affords the possibility of achieving amine termination by different synthetic routes, without the need for chemical protection. Second, the decrease in total conductance and the concomitant change in dG/dpH further support, by chemical reactivity, the successful installation, without chemical protection, of an at least partly amine-terminated layer during the photohydrosilylation step. Third, those same changes of conductance support the successful demonstration of click chemistry inside a SiN_x nanopore.

The nanopores functioned as chemically- and pH-tuned ionic conductors, capabilities with their own applications. We used the canonical nanopore demonstration molecule, λ -DNA, to test whether functionalization had deleteriously affected the use of the nanopores for translocation-based molecular sensing—simply put, whether the chemical functionalization had somehow obstructed the pores so that molecules could no longer pass through them. In addition to this key test, this measurement allowed us to explore the nature of the molecular signals from similarly-sized SiN_x (\sim 7.6 \pm 0.5 nm), Si-R-OH-functionalized (\sim 8.6 \pm 0.6 nm), and Si-R-NH₂-functionalized (\sim 10.7 \pm 0.7 nm) nanopores. Taken together, proof-of-principle evidence of translocation and whether the chemical coating properties affected translocation of this test molecule would be an

important foundational step in supporting further studies with additional variation of surface coating and electrolyte composition, and with a wider and more diverse analyte scope. We added λ-DNA at ~0.125 nM concentrations in 4 M LiCl electrolyte, ⁶¹⁻⁶² buffered at pH~7 with HEPES and applied a +600 mV voltage to drive electrophoretic passage of the anionic DNA through the nanopores. Current traces and scatter plots of measured λ -DNA current and conductance blockages are shown in Figure 3, along with histograms of instantaneous ΔG across all events, and histograms of event duration. Time-averaging of the open pore currents gave standard deviations of 162 pA (native SiN_x), 268 pA (Si-R-OH-functionalized), and 402 pA (Si-R-NH₂-functionalized). Power spectral densities of the same 5-second current traces are shown in Figure S-3. Regardless of surface functionalization, the signal-to-noise ratio is sufficient to permit straightforward detection of DNA translocations. The λ -DNA events were peaked at \sim 1.16 and 2.32 nS (bare SiN_x), \sim 1.54 and 3.22 nS (-OH-terminated), and \sim 1.89 and 3.85 nS (-NH₂-functionalized), with the \sim 2× factor between peaks consistent with passage of λ -DNA through the nanopore in linear and folded conformations.³⁹ We fit the first nonzero ΔG for each pore using Equation (4), with free $r_{\lambda-\mathrm{DNA}}$ and for L within the 10 ± 1.5 nm specified by the manufacturer. For bare, –OH-terminated, and – NH₂-terminated SiN_x nanopores, the resulting $d_{\lambda-DNA}$ (diameter of λ -DNA) ranged from 2.22– 2.28 nm (2.14-2.17 nm), 2.27-2.35 (2.17-2.21 nm), and 2.34-2.43 nm (2.21-2.26 nm) for values of L (and L_{eff} =L/2). These fit results (Figure S-4) were in good agreement with the reported hydrated diameter of 2.2-2.6 nm, ^{34, 63-64} and thus offered a conventional demonstration of the hydrosilylated nanopores as functional translocation-based molecular sensing elements, beyond their already demonstrated functional performance as pH-tuneable ionic conductors. Put more simply, photohydrosilylation-driven and subsequent chemical modifications did not obstruct the pores. Event durations (Table S-2) varied with surface functionalization (Figure 3, Figure S-5), with the

shortest events for the anionic λ -DNA measured in unfunctionalized SiN_x nanopores (~225 μ s), with a $\sim 1.5 \times$ increase with –OH-termination ($\sim 340 \mu s$), and a $> 5 \times$ increase with –NH₂-termination (\sim 1000 µs). The magnitude of these changes is comparable to the 4× tuning of translocation time achieved through pH-tuning of nanopore surface charge, ¹⁷ but here were obtained through covalent chemical modification without change of solution pH. The reduction, to a single parameter such as mean event time, is unlikely to delineate which of the panoply of mechanisms spanning electrostatics, electrokinetics, chemical interactions, and conformational dynamics, is active. The changes in that parameter with chemical coating does, however, illustrate that chemical tuning has had an influence on the nanopore sensing. The translocation time is affected by the interplay between surface charge density and polarity changes determining electrostatic and electroosmotic effects, ¹⁷ the effect of (electrolyte) lithium cation binding to the λ -DNA (slowing), ⁶¹ electrostatic shielding in the 4 M electrolyte, and even the nature of the interface—whether comprised of surface groups with a single charge polarity or mixed polarities (even if carrying the same overall charge), and whether the interface was at a condensed phase inorganic surface (SiN_x) or at an organic layer with presumably greater conformational flexibility (Si-R-OH, Si-R-NH₂). Event characteristics (in magnitude and time) show both biopolymer translocation and biopolymersurface-coating interactions, thus fulfilling the proof-of-principle purpose of the experiments. Current noise and event characteristics indicate the need to optimize the coatings and conditions for the desired application. Transit-time variability—particularly in response to electrolyte pH for example, has been reported in earlier DNA-translocation work using surface-functionalized pores, and was assigned to a predominantly electrostatic interaction. ¹⁷ Transient contacts between the translocating polymer and the nanopore coating would also broaden the translocation time distribution. Depending on nanopore surface functional group, interactions may include

chemically specific interactions between the surface and electrolyte ions (leading to possible effective surface charge neutralization, for example)⁶⁵ or between surface and analyte molecules, directly. The capability to tune nanopore surface chemistry as readily as has been outlined here, both in concert with and independent of solution pH changes, should allow for more detailed and systematic experiments designed to unravel such competing effects. The demonstration of chemical coating-specific changes to the λ -DNA signal characteristics bolsters the case for the use of the chemical functionalization method to tune nanopores for a much broader analyte scope encompassing, for example, proteins and glycans. The ability to exert molecular control over the size and solution interface of nanopore ionic circuit elements should also not be overlooked (Figure 2).

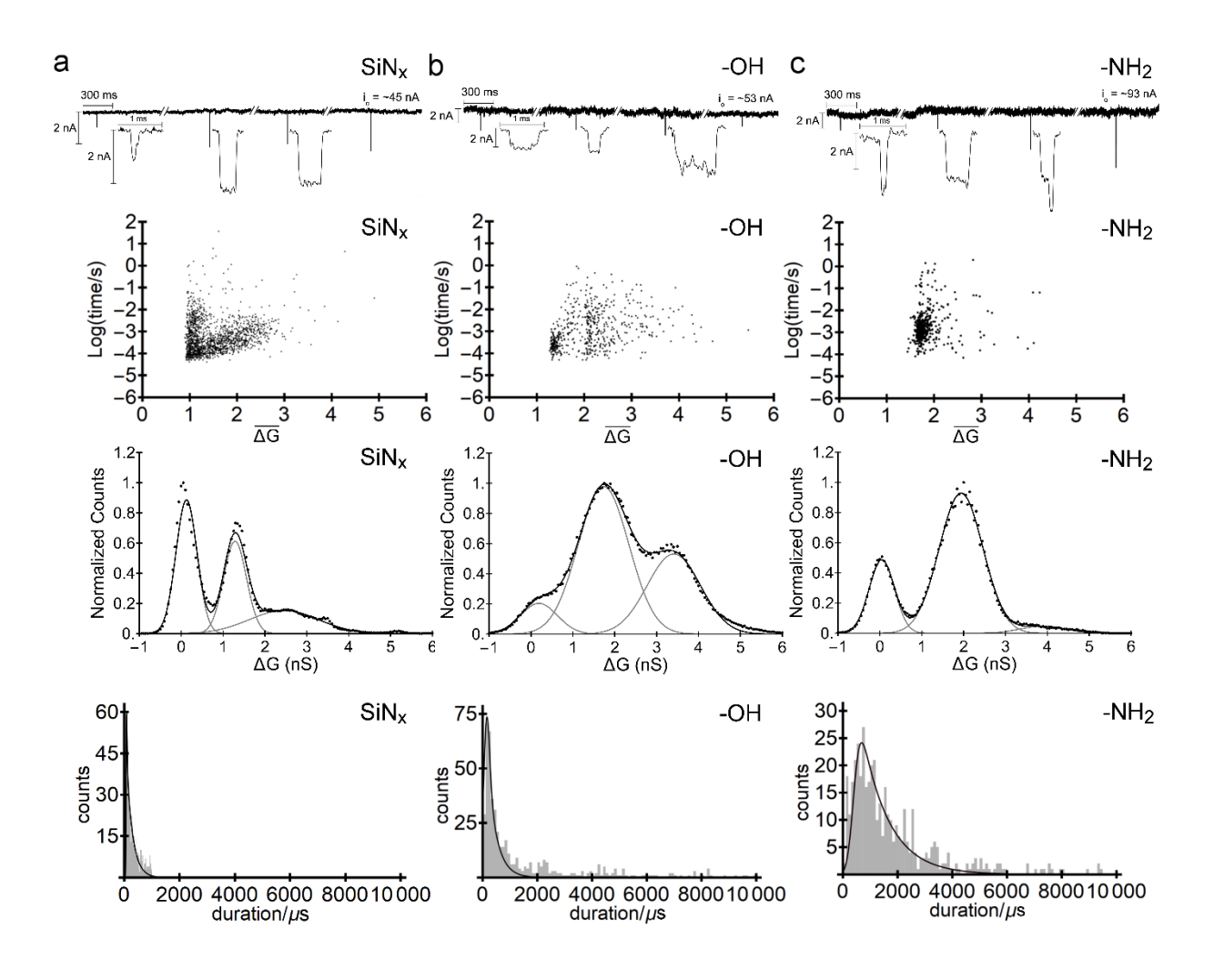


Figure 3. Detection of λ-DNA using chemically functionalized SiN_x nanopores in 4 M LiCl, 10 mM HEPES-buffered pH~7 electrolyte, recorded at 100 kHz acquisitions and 10 kHz low-pass filtering. Representations for translocation data of λ-DNA through a) bare (pore diameter ~7.6±0.5 nm) and b) 3-butene-ol hydrosylilated (pore diameter ~8.6±0.6 nm) and c) allylamine hydrosylilated (pore diameter ~10.7±0.7 nm) SiN_x nanopores. Row one: Sections of current traces in time with representative single events magnified. Row two: scatter plots for translocation duration with mean change in conductance per event ($\overline{\Delta G}$ (nS)). Row three: plots of instantaneous ΔG (nS) with normalized counts with the dashed grey traces corresponding to Gaussian fits, with the peaks at 0 nS corresponding to open-pore current levels bracketing those

of the measured blockages in the scatter plots. Row four: histogram of event number as a function of event duration, with the solid black traces corresponding to exponential fits (see Supporting Methods for details)

Conclusions.

We demonstrated that photohydrosilylation can be a robust and straightforward means of creating covalently surface-functionalized SiN_x nanopores. The use of controlled dielectric breakdown to form the nanopore eliminated the need—detrimental in the nanopore setting—for the hydrofluoric acid surface etching step necessary in conventional approaches. The initial organic layers tuned the effective nanopore size and altered the pH-responsive characteristics of these ionic solution conductors, allowing nanopore electrostatics and electrokinetics to be altered by covalent chemistry, solution pH tuning, or their combination, and affected the characteristics of nanopore sensing signals. These chemically-tailored nanopores could be further modified by drawing upon simple and powerful transformations such as condensation and click reactions, where click reactions occur quickly and in high yield under mild conditions and are a popular and accessible choice for installing biological moieties onto surfaces. The palette of chemical functionalization strategies demonstrated here thus has immediate application for creating chemically tuned pores, and promise as a foundation for creating biomimetic nanopores. The method dramatically increases the readily accessible parameter space for optimizing nanopore sensing including film thickness and film internal and terminal chemistry. In a broader sense, just CDB has democratized the formation of nanopore scaffolds, the etching-free (photo)hydrosilylation approach here has the potential to significantly broaden the adoption of bespoke chemically functionalized nanopores with attendant gains for wide-ranging application areas and implementations with a greater range of accessible analyte classes.

Methods

All electrical measurements were carried out using an Axopatch 200B amplifier (Axon Instruments, Foster City, CA, USA) in voltage clamp mode operated by custom coded Labview (National Instruments Corp., TX, USA) programs. All nanopores were formed by controlled dielectric breakdown (CDB)²⁷ (pH ~7, 1 M KCl, 10 mM HEPES) in free-standing nominally ~10 nm-thick low-pressure chemical vapour deposition (LPCVD) silicon-rich silicon nitride (SiN_x) membranes (each supplied with a manufacturer-specified thickness tolerance, ΔL). Conductance measurements—determined from a linear fit to the Ohmic current-voltage data from -200 to +200 mV—were used to analyze nanopore sizes, and size changes accompanying surface functionalization. Nanopore diameters were inferred from measurement of the conductance (pH \sim 7, 1 M KCl, 10 mM HEPES) using Equation (1), with σ calculated using Equation (3) and the parameters listed in Table S-1. For bare SiN_x, the conventional approach of considering only the acidic surface group at pH \sim 7 was followed.^{2, 28-30} Nanopore radii are reported as the value corresponding to the use of the 10 nm nominal membrane thickness, L, as the nanopore length in the calculation; the standard deviation of this radius and those calculated using $L - \Delta L$ and $L + \Delta L$ was reported as the uncertainty in the radius, thereby incorporating the tolerance in membrane thickness. The change of nanopore radius after each chemical treatment, δ , was reported as the intercept of the linear fit to a plot of r_0 versus $r_0 - \delta$ (Figure S-2), with the uncertainty in δ set equal to the standard error of the fit. The surface pK_a (Table S-1) was reported as the mean±(standard deviation) of the average of the individual fits to the G versus pH profiles for independent nanopores. Further details of the calculations, including data, are provided in the Supporting Methods.

All chemical reactions were carried out using as-supplied, commercially-obtained reagents: 3-butenen-1-ol (96%); adipoyl chloride (98%); allylamine (98%); 3,5-bis(trifluoromethyl)phenyl isocyanate (98%). Photohydrosilylation was carried out immediately (with no greater than 10 minutes allowed to elapse between pore formation and optical exposure) after nanopore formation, using a custom holder (Figure S-1) to hold the pore chip with neat liquid underneath a quartz plate. Conductance versus pH curves were constructed from measurements 15 minutes after each change of pH—from acidic to basic for acid pores, and the reverse order for basic pores. The solutions were comprised of 1 M KCl and 10 mM HEPES, and pH changes were driven by addition of hydrochloric acid or potassium hydroxide. The data for the functionalized pores were fit using Equations (1) and (3)—with *K* measured experimentally—to extract best-fit values for the surface pK_a (with suitable modifications for the pK_b). A sum of these two equations for acidic and basic pores was fit to G versus pH for the amphiprotic SiN_x pore and was used to determine its isoelectric point.

 λ -DNA was added to the *cis*- side of the nanopores (~0.125 nM with a 4 M LiCl electrolyte⁶⁰⁻⁶¹ buffered at pH~7) with a +600 mV applied potential applied to the *trans*- electrode consistent with electrophoretic travel of the anionic DNA through the nanopore to the *trans*- side (Figure 1). Transient changes to the current—blockages—detected in the presence of λ -DNA were extracted using a custom thresholding algorithm. Initial $i/\bar{\iota}_0$ –instantaneous/(time-averaged) open pore currents—edge detection thresholds of 0.972-0.979, 0.97-0.98, and 0.986 for SiN_x, Si-R-OH, and Si-R-NH₂ pores were used to identify events, followed by a refinement of the edge to $i/\bar{\iota}_0$ = 0.999. All events were individually quality-assured, and events exceeding 100 milliseconds were

rejected. Scatter plots of individual event characteristics show $\overline{\Delta G}$, where the conductance change was averaged across the event duration. Histograms of instantaneous ΔG were created using a 0.05 nS bin width across all extracted events, and include open pore conductances (ΔG peak centered at 0) bracketing each event.

A more detailed description of the materials and methods is supplied in the Supporting Information.

ASSOCIATED CONTENT

The following files are available free of charge.

Supporting Information. Detailed listing of materials and methods, and explanation of analyses. (PDF)

AUTHOR INFORMATION

Corresponding Author

*jason dwyer@uri.edu.

Present Addresses

† Department of Mechanical Engineering, Lyle School of Engineering, Southern Methodist University, Dallas, TX, 75275, United States.

Author Contributions

The manuscript was written through contributions of all authors. All authors have given approval to the final version of the manuscript.

Funding Sources

This research has been supported by NSF CAREER award CBET-1150085 and NSF award CHE-1808344, and by the University of Rhode Island, including URI graduate fellowships for Y. M. Nuwan D. Y. Bandara and Buddini Iroshika Karawdeniya.

ACKNOWLEDGMENT

This research has been supported by NSF CAREER award CBET-1150085 and NSF award CHE-1808344, and by the University of Rhode Island, including URI graduate fellowships for Y. M. Nuwan D. Y. Bandara and Buddini Iroshika Karawdeniya. We thank Louis W. Rogowski (SMU) for supplying MATLAB code to calculate the power spectral density.

ABBREVIATIONS

SiN_x, silicon-rich silicon nitride; CDB, controlled dielectric breakdown; LPCVD, low-pressure chemical vapour deposition.

REFERENCES

- 1. Shi, W.; Friedman, A. K.; Baker, L. A., Nanopore Sensing. *Anal. Chem.* **2017**, *89*, 157-188.
- 2. Dwyer, J. R.; Bandara, Y. M. N. D. Y.; Whelan, J. C.; Karawdeniya, B. I.; Nichols, J. W., Silicon Nitride Thin Films for Nanofluidic Device Fabrication. In *Nanofluidics, 2nd Edition*, 2 ed.; Edel, J.; Ivanov, A.; Kim, M., Eds. Royal Society for Chemistry: **2016**; Chapter 7.
- 3. Harms, Z. D.; Haywood, D. G.; Kneller, A. R.; Jacobson, S. C., Conductivity-Based Detection Techniques in Nanofluidic Devices. *Analyst* **2015**, *140*, 4779-4791.

- 4. Taniguchi, M., Selective Multidetection Using Nanopores. *Anal. Chem.* **2015**, *87*, 188-199.
- 5. Miles, B. N.; Ivanov, A. P.; Wilson, K. A.; Dogan, F.; Japrung, D.; Edel, J. B., Single Molecule Sensing with Solid-State Nanopores: Novel Materials, Methods, and Applications. *Chem. Soc. Rev.* **2013**, *42*, 15-28.
- 6. Howorka, S.; Siwy, Z., Nanopore Analytics: Sensing of Single Molecules. *Chem. Soc. Rev.* **2009**, *38*, 2360-2384.
- 7. Siwy, Z. S.; Howorka, S., Engineered Voltage-Responsive Nanopores. *Chem. Soc. Rev.* **2010**, *39*, 1115-1132.
- 8. Tabard-Cossa, V.; Wiggin, M.; Trivedi, D.; Jetha, N. N.; Dwyer, J. R.; Marziali, A., Single-Molecule Bonds Characterized by Solid-State Nanopore Force Spectroscopy. *ACS Nano* **2009**, *3*, 3009-3014.
- 9. Hornblower, B.; Coombs, A.; Whitaker, R. D.; Kolomeisky, A.; Picone, S. J.; Meller, A.; Akeson, M., Single-Molecule Analysis of DNA-Protein Complexes Using Nanopores. *Nature Methods* **2007**, *4*, 315-317.
 - 10. Daiguji, H., Ion Transport in Nanofluidic Channels. Chem. Soc. Rev. 2010, 39, 901-911.
- 11. Schoch, R. B.; Han, J.; Renaud, P., Transport Phenomena in Nanofluidics. *Reviews of Modern Physics* **2008**, *80*, 839-883.
- 12. Karawdeniya, B. I.; Bandara, Y. M. N. D. Y.; Nichols, J. W.; Chevalier, R. B.; Dwyer, J. R., Surveying Silicon Nitride Nanopores for Glycomics and Heparin Quality Assurance. *Nat Commun* **2018**, *9*, 3278.

- 13. Wei, R.; Pedone, D.; Zürner, A.; Döblinger, M.; Rant, U., Fabrication of Metallized Nanopores in Silicon Nitride Membranes for Single-Molecule Sensing. *Small* **2010**, *6*, 1406-1414.
- 14. Wanunu, M.; Meller, A., Chemically Modified Solid-State Nanopores. *Nano Lett.* **2007,** 7, 1580-1585.
- 15. Yusko, E. C.; Johnson, J. M.; Majd, S.; Prangkio, P.; Rollings, R. C.; Li, J.; Yang, J.; Mayer, M., Controlling Protein Translocation through Nanopores with Bio-Inspired Fluid Walls. *Nat Nanotechnol* **2011**, *6*, 253-260.
- 16. Lepoitevin, M.; Ma, T.; Bechelany, M.; Janot, J.-M.; Balme, S., Functionalization of Single Solid State Nanopores to Mimic Biological Ion Channels: A Review. *Adv. Colloid Interface Sci.* **2017**, *250*, 195-213.
- 17. Anderson, B. N.; Muthukumar, M.; Meller, A., Ph Tuning of DNA Translocation Time through Organically Functionalized Nanopores. *ACS Nano* **2012**, *7*, 1408-1414.
- 18. Nguyen, A. T.; Baggerman, J.; Paulusse, J. M. J.; van Rijn, C. J. M.; Zuilhof, H., Stable Protein-Repellent Zwitterionic Polymer Brushes Grafted from Silicon Nitride. *Langmuir* **2011**, *27*, 2587-2594.
- 19. Rosso, M.; Giesbers, M.; Arafat, A.; Schroën, K.; Zuilhof, H., Covalently Attached Organic Monolayers on SiC and Si_xN₄ Surfaces: Formation Using UV Light at Room Temperature. *Langmuir* **2009**, *25*, 2172-2180.
- 20. Arafat, A.; Giesbers, M.; Rosso, M.; Sudhölter, E. J. R.; Schroën, K.; White, R. G.; Yang, L.; Linford, M. R.; Zuilhof, H., Covalent Biofunctionalization of Silicon Nitride Surfaces. *Langmuir* **2007**, *23*, 6233-6244.

- 21. Arafat, A.; Schroën, K.; de Smet, L. C. P. M.; Sudhölter, E. J. R.; Zuilhof, H., Tailor-Made Functionalization of Silicon Nitride Surfaces. *J. Am. Chem. Soc.* **2004**, *126*, 8600-8601.
- 22. Nguyen, A. T.; van Doorn, R.; Baggerman, J.; Paulusse, J. M. J.; Klerks, M. M.; Zuilhof, H.; van Rijn, C. J. M., Flow-through Microbial Capture by Antibody-Coated Microsieves. *Advanced Materials Interfaces* **2015**, *2*, 1400292-n/a.
- 23. Kolb, H. C.; Finn, M. G.; Sharpless, K. B., Click Chemistry: Diverse Chemical Function from a Few Good Reactions. *Angewandte Chemie International Edition* **2001**, *40*, 2004-2021.
- 24. Escorihuela, J.; Marcelis, A. T. M.; Zuilhof, H., Metal-Free Click Chemistry Reactions on Surfaces. *Advanced Materials Interfaces* **2015**, *2*, 1500135-n/a.
- 25. Rosso, M.; Nguyen, A. T.; de Jong, E.; Baggerman, J.; Paulusse, J. M. J.; Giesbers, M.; Fokkink, R. G.; Norde, W.; Schroën, K.; Rijn, C. J. M. v.; Zuilhof, H., Protein-Repellent Silicon Nitride Surfaces: UV-Induced Formation of Oligoethylene Oxide Monolayers. *ACS Appl. Mater. Interfaces* **2011**, *3*, 697-704.
- 26. Firnkes, M.; Pedone, D.; Knezevic, J.; Döblinger, M.; Rant, U., Electrically Facilitated Translocations of Proteins through Silicon Nitride Nanopores: Conjoint and Competitive Action of Diffusion, Electrophoresis, and Electroosmosis. *Nano Lett.* **2010**, *6*, 895-909.
- 27. Kwok, H.; Briggs, K.; Tabard-Cossa, V., Nanopore Fabrication by Controlled Dielectric Breakdown. *PLoS ONE* **2014**, *9*, e92880.
- 28. Bandara, Y. M. N. D. Y.; Nichols, J. W.; Iroshika Karawdeniya, B.; Dwyer, J. R., Conductance-Based Profiling of Nanopores: Accommodating Fabrication Irregularities. *Electrophoresis* **2018**, *39*, 626-634.

- 29. Smeets, R. M. M.; Keyser, U. F.; Krapf, D.; Wu, M.-Y.; Dekker, N. H.; Dekker, C., Salt Dependence of Ion Transport and DNA Translocation through Solid-State Nanopores. *Nano Lett.* **2006**, *6*, 89-95.
- 30. Liebes, Y.; Drozdov, M.; Avital, Y. Y.; Kauffmann, Y.; Rapaport, H.; Kaplan, W. D.; Ashkenasy, N., Reconstructing Solid State Nanopore Shape from Electrical Measurements. *Appl. Phys. Lett.* **2010**, *97*, 223105.
- 31. Hoogerheide, D. P.; Garaj, S.; Golovchenko, J. A., Probing Surface Charge Fluctuations with Solid-State Nanopores. *Phys. Rev. Lett.* **2009**, *102*, 256804.
- 32. Detcheverry, F.; Bocquet, L., Thermal Fluctuations in Nanofluidic Transport. *Phys. Rev. Lett.* **2012**, *109*, 024501.
- 33. Ayub, M.; Ivanov, A.; Instuli, E.; Cecchini, M.; Chansin, G.; McGilvery, C.; Hong, J.; Baldwin, G.; McComb, D.; Edel, J. B.; Albrecht, T., Nanopore/Electrode Structures for Single-Molecule Biosensing. *Electrochim. Acta* **2010**, *55*, 8237-8243.
- 34. Kowalczyk, S. W.; Grosberg, A. Y.; Rabin, Y.; Dekker, C., Modeling the Conductance and DNA Blockade of Solid-State Nanopores. *Nanotechnology* **2011**, *22*, 315101.
- 35. Lee, C.; Joly, L.; Siria, A.; Biance, A.-L.; Fulcrand, R.; Bocquet, L., Large Apparent Electric Size of Solid-State Nanopores Due to Spatially Extended Surface Conduction. *Nano Lett.* **2012**, *12*, 4037-4044.
- 36. Behrens, S. H.; Grier, D. G., The Charge of Glass and Silica Surfaces. *J. Chem. Phys.* **2001**, *115*, 6716-6721.

- 37. Jiang, Z.; Stein, D., Charge Regulation in Nanopore Ionic Field-Effect Transistors. *Physical Review E* **2011**, *83*, 031203.
- 38. van Dorp, S.; Keyser, U. F.; Dekker, N. H.; Dekker, C.; Lemay, S. G., Origin of the Electrophoretic Force on DNA in Solid-State Nanopores. *Nature Physics* **2009**, *5*, 347-351.
- 39. Li, J.; Gershow, M.; Stein, D.; Brandin, E.; Golovchenko, J. A., DNA Molecules and Configurations in a Solid-State Nanopore Microscope. *Nature Materials* **2003**, *2*, 611-615.
- 40. Kasianowicz, J. J.; Nguyen, T. L.; Stanford, V. M., Enhancing Molecular Flux through Nanopores by Means of Attractive Interactions. *P Natl Acad Sci USA* **2006**, *103*, 11431-11432.
- 41. Maglia, G.; Restrepo, M. R.; Mikhailova, E.; Bayley, H., Enhanced Translocation of Single DNA Molecules through A-Hemolysin Nanopores by Manipulation of Internal Charge. *P Natl Acad Sci USA* **2008**, *105*, 19720-19725.
- 42. Mohammad; Prakash, S.; Matouschek, A.; Movileanu, L., Controlling a Single Protein in a Nanopore through Electrostatic Traps. *J. Am. Chem. Soc.* **2008**, *130*, 4081-4088.
- 43. Wong, C. T. A.; Muthukumar, M., Polymer Translocation through Alpha-Hemolysin Pore with Tunable Polymer-Pore Electrostatic Interaction. *The Journal of Chemical Physics* **2010**, *133*, 045101-045112.
- 44. Sexton, L. T.; Horne, L. P.; Martin, C. R., Developing Synthetic Conical Nanopores for Biosensing Applications. *Molecular BioSystems* **2007**, *3*, 667-685.
- 45. Gyurcsányi, R. E., Chemically-Modified Nanopores for Sensing. *TrAC, Trends Anal. Chem.* **2008,** *27*, 627-639.

- 46. Wei, R.; Gatterdam, V.; Wieneke, R.; Tampe, R.; Rant, U., Stochastic Sensing of Proteins with Receptor-Modified Solid-State Nanopores. *Nat Nano* **2012**, *7*, 257-263.
- 47. Karawdeniya, B. I.; Bandara, Y. M. N. D. Y.; Nichols, J. W.; Chevalier, R. B.; Hagan, J. T.; Dwyer, J. R., Challenging Nanopores with Analyte Scope and Environment. *Journal of Analysis and Testing* **2019**, *3*, 61-79.
- 48. Dwyer, J. R.; Harb, M., Through a Window, Brightly: A Review of Selected Nanofabricated Thin-Film Platforms for Spectroscopy, Imaging, and Detection. *Appl. Spectrosc.* **2017,** *71*, 2051-2075.
- 49. Feng, Z.; Emma, L.; Faheem, A.; Pilar, R. G.; Fang, Y.; Paul, M.; J., P. W., Polymer-Coated Nanoparticles: A Universal Tool for Biolabelling Experiments. *Small* **2011**, *7*, 3113-3127.
- 50. Munakata, H.; Kuwabata, S., Detection of Difference in Acidity between Arrayed Carboxy Groups and the Groups Dissolved in Solution by Reductive Desorption of a Self-Assembled Monolayer of Carboxy-Terminated Thiols. *Chemical Communications* **2001**, 1338-1339.
- 51. Schweiss, R.; Welzel, P. B.; Werner, C.; Knoll, W., Dissociation of Surface Functional Groups and Preferential Adsorption of Ions on Self-Assembled Monolayers Assessed by Streaming Potential and Streaming Current Measurements. *Langmuir* **2001**, *17*, 4304-4311.
- 52. van der Vegte, E. W.; Hadziioannou, G., Acid-Base Properties and the Chemical Imaging of Surface-Bound Functional Groups Studied with Scanning Force Microscopy. *The Journal of Physical Chemistry B* **1997**, *101*, 9563-9569.
- 53. Holmes-Farley, S. R.; Bain, C. D.; Whitesides, G. M., Wetting of Functionalized Polyethylene Film Having Ionizable Organic Acids and Bases at the Polymer-Water Interface:

Relations between Functional Group Polarity, Extent of Ionization, and Contact Angle with Water. *Langmuir* **1988**, *4*, 921-937.

- 54. Vezenov, D. V.; Noy, A.; Rozsnyai, L. F.; Lieber, C. M., Force Titrations and Ionization State Sensitive Imaging of Functional Groups in Aqueous Solutions by Chemical Force Microscopy. *J. Am. Chem. Soc.* **1997**, *119*, 2006-2015.
- 55. Zhao, B.; Mulkey, D.; Brittain, W. J.; Chen, Z.; Foster, M. D., Synthesis and Characterization of Phenol- and O-Chlorophenol-Terminated Monolayers. *Langmuir* **1999**, *15*, 6856-6861.
- 56. Wang, B.; Abdulali-Kanji, Z.; Dodwell, E.; Horton, J. H.; Oleschuk, R. D., Surface Characterization Using Chemical Force Microscopy and the Flow Performance of Modified Polydimethylsiloxane for Microfluidic Device Applications. *Electrophoresis* **2003**, *24*, 1442-1450.
- 57. Marmisollé, W. A.; Capdevila, D. A.; de la Llave, E.; Williams, F. J.; Murgida, D. H., Self-Assembled Monolayers of Nh2-Terminated Thiolates: Order, Pka, and Specific Adsorption. *Langmuir* **2013**, *29*, 5351-5359.
- 58. Sheikh, K. H.; Evans, S. D.; Christenson, H. K., Titration of Ionizable Monolayers by Measurement of the Electric Double-Layer Force. *Langmuir* **2007**, *23*, 6893-6895.
- 59. Sieval, A. B.; Linke, R.; Heij, G.; Meijer, G.; Zuilhof, H.; Sudhölter, E. J. R., Amino-Terminated Organic Monolayers on Hydrogen-Terminated Silicon Surfaces. *Langmuir* **2001**, *17*, 7554-7559.

- 60. Crc Handbook of Chemistry and Physics. 99 (Internet Version 2018) ed.; CRC Press/Taylor & Francis: Boca Raton, FL, **2018**.
- 61. Kowalczyk, S. W.; Wells, D. B.; Aksimentiev, A.; Dekker, C., Slowing Down DNA Translocation through a Nanopore in Lithium Chloride. *Nano Lett.* **2012**, *12*, 1038-1044.
- 62. Plesa, C.; Verschueren, D.; Pud, S.; van der Torre, J.; Ruitenberg, J. W.; Witteveen, M. J.; Jonsson, M. P.; Grosberg, A. Y.; Rabin, Y.; Dekker, C., Direct Observation of DNA Knots Using a Solid-State Nanopore. *Nat Nanotechnol* **2016**, *11*, 1093-1097.
- 63. Douglas, S. M.; Dietz, H.; Liedl, T.; Högberg, B.; Graf, F.; Shih, W. M., Self-Assembly of DNA into Nanoscale Three-Dimensional Shapes. *Nature* **2009**, *459*, 414.
- 64. Tirado, M. M.; Martínez, C. L.; Torre, J. G. d. l., Comparison of Theories for the Translational and Rotational Diffusion Coefficients of Rod-Like Macromolecules. Application to Short DNA Fragments. *The Journal of Chemical Physics* **1984**, *81*, 2047-2052.
- 65. Siwy, Z. S.; Powell, M. R.; Kalman, E.; Astumian, R. D.; Eisenberg, R. S., Negative Incremental Resistance Induced by Calcium in Asymmetric Nanopores. *Nano Lett.* **2006**, *6*, 473-477.

TOC Image

